crystals

MDPI

Article

Grain Refinement and Strengthening of an Aluminum Alloy Subjected to Severe Plastic Deformation through Equal-Channel Angular Pressing

Atef Korchef * and Imen Souid

College of Sciences, King Khalid University (KKU), P.O. Box 9004, Abha 61413, Saudi Arabia
* Correspondence: akorchef@kku.edu.sa

Abstract: In the present study, the microstructure, mechanical properties, and stored energy of an aluminum alloy containing iron-rich fine precipitates, subjected to severe plastic deformation through equal-channel angular pressing (ECAP), were investigated using X-ray diffraction, scanning electron microscopy, transmission electron microscopy, and atomic force microscopy. Up to four passes through ECAP resulted in significant nanometer-scale grain refinement, as well as the accumulation of lattice defects, such as dislocations and mesoscopic shear planes. This resulted in a noticeable enhancement in the Vickers microhardness and the flow stress after ECAP. Differential scanning calorimetry results showed that the ECAP'ed material exhibited two exothermal peaks at 222 ± 2 °C and 362 ± 2 °C, with total thermal effects of ΔH = 4.35 and 6.5 J/g, respectively. Slight increases in the ECAP'ed material microhardness and flow stress were observed at 200 °C. The heat release, at a relatively low temperature, and the slight improvement in the mechanical properties were attributed to the evolution of low- and high-angle misorientation, with the strain and the pinning of tangled dislocation caused by the existing fine particles. The second peak was attributed to grain growth, resulting in a significant softening of the material.

Keywords: ECAP; aluminum alloy; microstructure; mechanical properties; heat release; grain refinement

Citation: Korchef, A.; Souid, I. Grain Refinement and Strengthening of an Aluminum Alloy Subjected to Severe Plastic Deformation through Equal-Channel Angular Pressing. *Crystals* **2023**, *13*, 1160. https://doi.org/10.3390/cryst13081160

Academic Editor: Hongbin Bei

Received: 19 June 2023
Revised: 18 July 2023
Accepted: 20 July 2023
Published: 26 July 2023

1. Introduction

In order to refine grains with moderate-to-high strain, numerous severe plastic deformation (SPD) processes have been utilized, including torsion under high pressure [1–3], ball milling [4,5], and equal-channel angular pressing (ECAP) [6–9]. During ECAP, the bulk of the sample undergoes approximately simple shear, and repetitive passes of the same sample can be achieved, since the sample cross-section remains unaltered after each pass. It was shown that the number of pressing cycles and the processing route strongly affect the microstructure and mechanical properties of ECAP'ed materials [10,11]. Metals and alloys deformed by ECAP showed heterogeneous microstructures, containing high-energy grain boundaries [12,13] or homogenous microstructures [14–16]. Indeed, the nature of the microstructure (homogeneous or heterogeneous) depends on the deformed material and the operating parameters of the ECAP. Nakashima et al. [17] conducted ECAP experiments on pure aluminum (99.99%) using protocol B (i.e., the sample was rotated by 90° between two successive passes through the die). They found that after the first pass, the microstructure consisted of elongated subgrain bands, approximately parallel to the upper and lower faces of the pressed sample. The subgrains were separated by low-angle boundaries. After two passes, the banded structure was less detectable, and the grains appeared more equiaxed. After four passes, the grains were equiaxed and separated by high-angle boundaries. The average grain size achieved was about 1.3 μm. Comparable results were found by Kawasaki et al. [18]. Indeed, they examined the microstructure of high-purity aluminum (99.99%) processed using ECAP through 1–12 passes. They found that the microstructure

evolved from elongated subgrains to an essentially equiaxed array of ultrafine grains, and both the boundary misorientation angle and fraction of high-angle boundaries increased rapidly from 1 to 4 passes. From 4 to 12 passes, there was no measurable change in the average grain size. Optimum processing was achieved using ECAP through 4–8 passes. The resulting texture depends on the strain accumulated during ECAP and the strain path changes involved in the ECAP process. Skrotzki et al. [19] investigated the texture of aluminum alloy AA 5109, deformed using ECAP at room temperature through three passes, without rotation between two successive passes (so-called route A). They showed that the resulting texture was characterized by typical shear components of FCC metals that deviate from their ideal positions, and it depended on several factors, such as the starting texture, the distance from the top of the extruded billet, and changes from pass to pass.

ECAP, among other techniques of SPD, has been applied to bulk metals and alloys in order to intensively refine their structures and enhance their mechanical properties. High dislocation density and fine grains with sizes less than 100 nm can typically be achieved, and, more generally, grains with sizes in the submicrometer range were produced using ECAP [20,21]. As a result, the mechanical properties of ultrafine-grained (UFG) materials are significantly improved, compared to those of coarse-grained materials. Several UFG materials, including aluminum alloys, for instance, were found to exhibit superplastic behavior, enhanced flow stress, and high Vickers microhardness [22–24]. Mabuchi and Higashi [25] investigated the mechanical properties of a relatively low-purity Al (99.5%) and a high-purity Al (99.9999%) deformed using ECAP at room temperature. They showed that the tensile strength of Al (99.5%) was improved after ECAP, and this improvement depended on impurities and temperature. The tensile strength increased up to a total strain of 7.3, and then it remained constant for higher values. In addition, the flow stress decreased for a strain of 7.3 and remained unchanged for larger strains. For Al (99.9999%), the tensile strength was poorly improved after ECAP because of the dislocation restoration, which readily occurs below room temperature. Verlinden and Popović [26] studied the mechanical properties of free copper Al-4.4 wt% Mg and AA5182 containing 1.2 wt% Cu Alloys after four and eight ECAP passes at 200 °C. They showed that the addition of copper to the alloy increased the strength of the alloy by 20%. Post-ECAP annealing at 200 °C did not lead to further increases in hardness or strength. Indeed, the precipitates formed during ECAP at 200 °C did not directly contribute to the higher strength of the copper-rich alloy, but they slowed down the recovery.

When the temperature increases, UFG materials become softer in both their plastic and elastic regimes [27]. The changes in the elastic parameters were attributed to a change in the grain boundary, leading to important changes in the microhardness and yield stress [28]. Furthermore, UFG materials may display superplastic properties at relatively low temperatures, owing to the enhancement of grain boundary diffusion processes [29]. The models by Lifshitz [30] and Rachinger [31] describe deformation processes via grain boundary sliding (GBS) in conventional polycrystals under diffusion creep and dislocation creep, at high temperatures or superplastic conditions, respectively. Hahn et al. [28] proposed an alternative deformation model for UFG materials, based on GBS and the formation of mesoscopic shear planes. In this model, at a critical grain size, a transition from plastic deformation, dominated by dislocation, to GBS arises when the stress needed for the formation and motion of dislocation becomes higher than that needed for GBS. Consequently, the Hall–Petch relationship, which states that a material becomes harder when its grains become smaller, remains valid for some nanocrystalline materials [23,32], which is consistent with a high-angle grained structure; however, a negative slope (the inverse Hall–Petch relationship) was found in some cases of hardness measurements [33,34]. Different assumptions and models were proposed with which to explain this unusual behavior, such as the precipitation of a second phase in grain boundaries [28], a sliding of grain boundaries and formation of mesoscopic shear planes [32], and an extrinsic dislocation movement in the non-equilibrium grain boundaries when hardness measurements were taken [35].

Different techniques have been used to observe the microstructure evolution of UFG metals and alloys during the ECAP process, i.e., transmission electron microscopy (TEM), optical microscopy (OM), and X-ray diffraction (XRD). Atomic force microscopy (AFM) can be used with these techniques to give further experimental information about the microstructure and deformation mechanisms of UFG materials. However, it seems that only a few studies used AFM to investigate the microstructure of materials processed by ECAP [36,37]. AFM can be extremely useful to study the deformation mechanisms after mechanical tests of materials processed by ECAP. For example, using AFM, it was shown that the dominant deformation mechanism of nanostructured copper [38] was the dislocation-dominated plasticity and nano-void formation. In addition, AFM observations were carried out to determine the mechanism of fatigue damage in UFG copper processed by ECAP [39]. It was found that the strains initiated in UFG copper at the slip's edges caused the rotation of grains and the deformation in the adjacent nanometric grains. This resulted in the coarsening of the grains in the order of micrometers followed by the propagation of the slips. Also, an AFM investigation confirmed the transition in deformation mechanisms with decreasing strain rate and provide irrefutable evidence for the existence of GBS within the superplastic regime for Zn-22% Al eutectoid samples processed by ECAP at a temperature of 200 °C and pulled to strains in the range ~0.2–0.5 [40].

The present work aims to Investigate the microstructure and mechanical properties of aluminum that contains an iron-rich α-phase situated essentially at grain boundaries during ECAP. The material used in our work is low-purity recycled aluminum (99.1%). Unlike high-purity aluminum, it is cheap and easy to obtain at an industrial scale. Also, a major problem encountered when using UFG materials at high temperatures is the coarsening of their grains which negatively affected their mechanical properties. However, the presence of the α-phase in the aluminum matrix was expected to improve the thermal stability of the processed material. This is of utmost importance for industrial applications of the ECAP'ed aluminum alloy at relatively high temperatures. For this purpose, OM, SEM, TEM, and XRD were used for microstructure investigation. A complementary investigation on the microstructure, in particular the formation of mesoscopic shear planes, was carried out using AFM.

Tension and Vickers microhardness measurements were performed for the mechanical tests. The effect of annealing on the hardening of the alloy was then investigated using Vickers microhardness and tensile tests. Stored energy measurements were performed using differential scanning calorimetry (DSC).

2. Materials and Methods

Experiments were performed on an aluminum alloy containing 0.2 wt% Fe, 0.1 wt% Si, 0.17 wt% Mg, 0.15 wt% Zn, and 0.07% Mn, and Al was the balance. The aluminum alloy, received in the form of cast ingots, was annealed at 500 °C for 24 h and then quenched in iced water. After annealing, the microstructure of the alloy consisted of large grains (~80 µm in size) (Figure 1a). Thereafter, samples with a square section (10 × 10 mm^2) and 70 mm in length were cut for ECAP. Prior to ECAP, the samples were coated with lithium-based lubricant. The aluminum matrix contained fine and coarse precipitates (with a volume fraction of ~1%) most of which were situated at grain boundaries (Figure 1b). Analysis via X-ray emission spectrometry indicated that these precipitates contain Al, Fe, and Si (Figure 1c). The possible chemistry of this phase, usually denoted as α-AlFeSi, is $Al_{12}Fe_3Si$ or $Al_{15}Fe_3Si_2$.

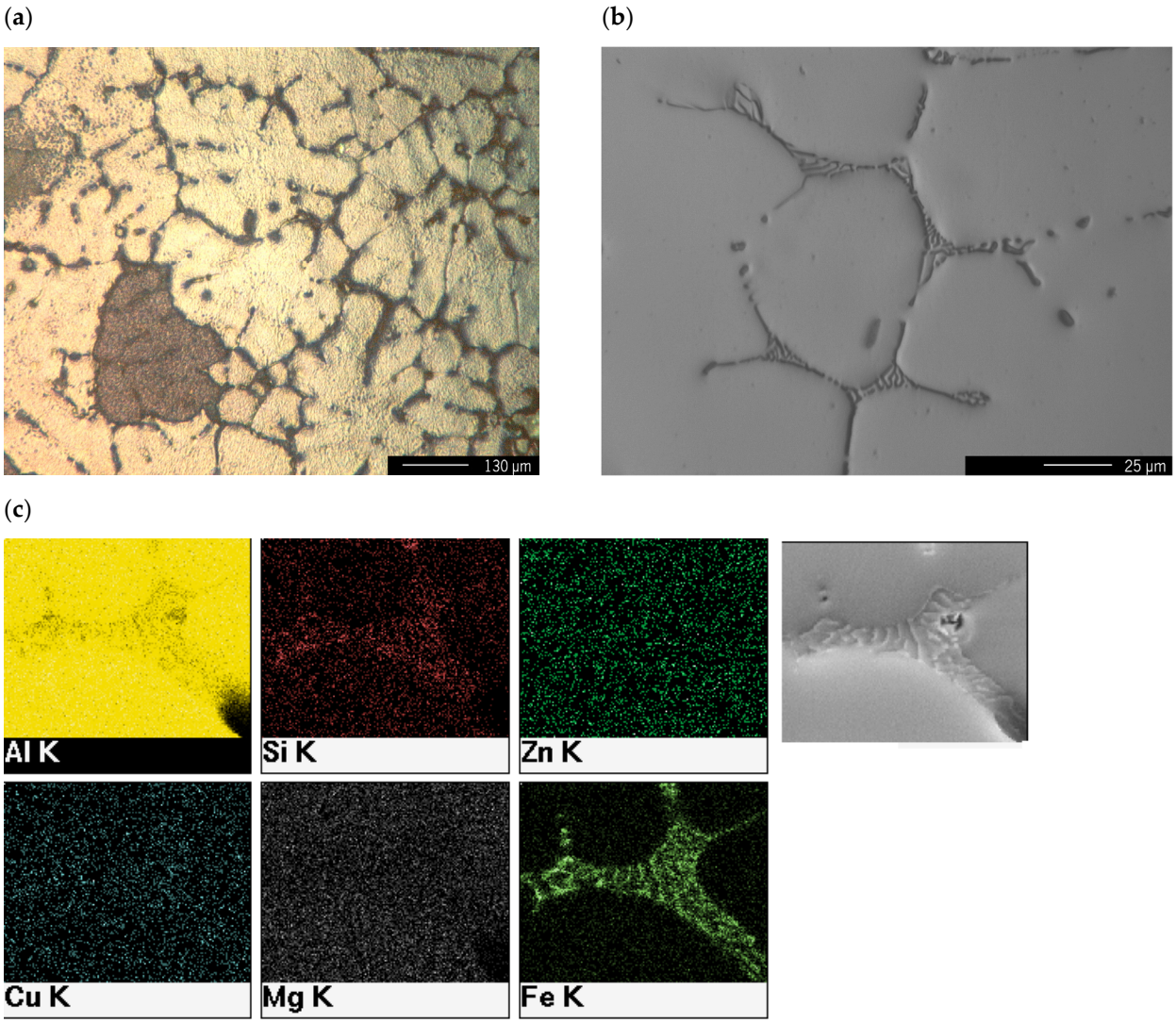

Figure 1. (**a**) Optical micrograph under polarized light of the nondeformed (N = 0) sample. (**b**) SEM micrograph and (**c**) X-ray emission spectrometry via SEM of the fine precipitates in the aluminum matrix.

The surfaces of the samples were ground mechanically and polished electrolytically for 30 min at temperatures less than 10 °C under a 30 V operating voltage in a solution of 66% $(CH_3CO)_2O$ and 34% $HClO_4$. Samples were subjected to high strains through ECAP. The ECAP die used in the present work consisted of two square channels with a cross-sectional area of 10 × 10 mm^2 each, which met at an angle Ø = 90°. An angle ψ = 20° was delineated by the curvature arc at the outer point of the intersection of the two square channels (Figure 2). Since the cross-section of the sample remained the same after each pass through the die during the ECAP procedure, it was possible to repeatedly press the same sample to attain high strains. Using the formula provided by Iwahashi et al. [41], the sample was subjected to an equivalent strain, ε_N, equal to ~N after N passes through the die. In the present study, the same sample was repeatedly pressed in the same direction after each pass (the so-called route A) through the die to reach an equivalent strain of up to ~4.

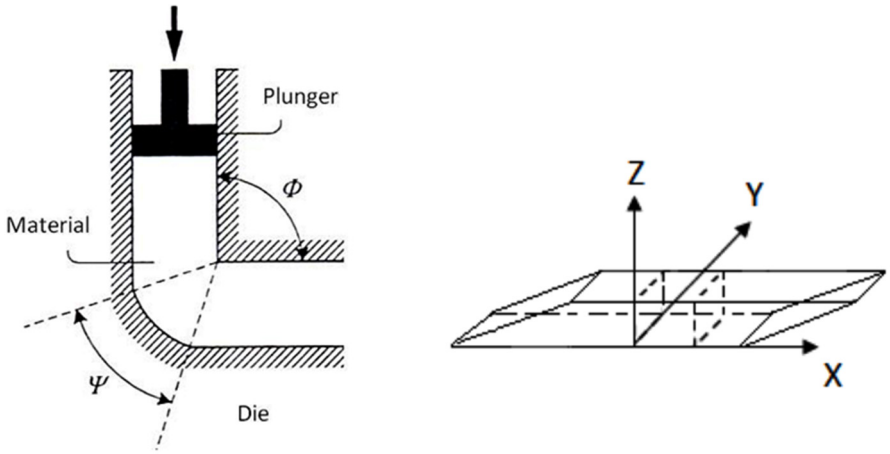

Figure 2. Schematic illustrations of the ECAP die (**left**) and the sample shape after ECAP (**right**). The *X*-axis is the pressing direction.

A Philips X'PERT PRO diffractometer (Malvern Panalytical, Malvern, United Kingdom) was used to perform XRD patterns in step scanning mode with the radiation Co-Kα. The XRD patterns were recorded at room temperature in the scanning range 2θ between 30 and 155° at a scan rate of 2×10^{-3} deg/s. The APD 1700 software (Philips, Amsterdam, Netherlands) was used to determine the full width at half maximum (FWHM) of each reflection. The following expression was used to obtain a correction for the instrumental effects' contribution to the experimental FWHM, ßexp, for each reflection:

$$ß = ([(ß^2)_{exp} - (ß^2)_{ins}]^{1/2} \times [ß_{exp} - ß_{ins}])^{1/2} \quad (1)$$

where $ß_{ins}$ is the instrumental FWHM determined using the nondeformed (N = 0) aluminum alloy as standard reference material. The Halder–Wagner (HW) method, which assumes a Voigt peak shape, was used to calculate the microstrains (lattice distortions) and the crystallite size of the ECAP'ed samples [42]:

$$(\beta^*/d^*)^2 = 1/D[\beta^*/(d^*)^2] + (\varepsilon/2)^2 \quad (2)$$

where $\beta^* = \beta \cos\theta/\lambda$ and $d^* = 2 \sin\theta/\lambda$; θ is the Bragg angle, and λ is the wavelength used. From Equation (2), the slope gives the crystallite size, and the intercept of the plot of $(\beta^*/d^*)^2$ versus $\beta^*/(d^*)^2$ gives the value of the microstrains.

Dislocations are the main defects in SPD samples, and considering that the nondeformed sample was submitted to a prolonged annealing at the high temperature of 500 °C, one can assume that the dislocation density of the nondeformed sample, ρ_i, was significantly lower than the dislocation density,]ρ, accumulated after ECAP ($\rho_i << \rho$). In that case, ρ can be estimated by the following equation [43]:

$$\rho = \frac{1}{D\left(y + \frac{b}{\varepsilon_N}\right)} \quad (3)$$

In this equation, D is the crystallite size calculated from the reflection broadening, $\varepsilon_N = N$ is the strain introduced by ECAP, b is the magnitude of the Burgers vector of dislocation ($b = a/\sqrt{2}$ for FCC aluminum alloys, where a is the aluminum lattice parameter), and y is the annihilation distance of dislocation (y = 2 nm).

The surface topographies of samples deformed by ECAP were observed using a scanning electron microscope operating at 25 kV and a Digital instruments Nanoscope III atomic force microscope operating in the tapping mode.

A DURIMET microhardness tester, with a diamond pyramidal indenter, was used for the Vickers microhardness, H_V, measurements. Eight measurements were taken with

a load of 100 g applied at randomly selected points for 15 s. Cylindric specimens with dimensions of 15 mm and 3 mm for the gage length and gage diameters, respectively, were cut along the *X*-axis for tensile tests. Tensile tests were performed at room temperature, using an Instron testing machine, at a crosshead displacement speed of 0.05 mm.min^{-1} (equivalent to an initial strain rate of 5.5×10^{-5} s^{-1}).

In order to investigate a possible recovery, four-pass (N = 4) specimens were annealed for 1 h at temperatures between 25 and 400 °C. Then, XRD analysis, Vickers microhardness measurements, and tensile tests were performed on each sample.

A Perkin Elmer calorimeter was used for differential scanning calorimetry (DSC) measurements. The material was heated at a rate of 40 °C·min^{-1} in closed copper crucibles. Three heating runs on the same sample were accomplished under an argon atmosphere from room temperature up to 600 °C. The two last runs were used to determine the baseline. The DSC experiments were performed on three samples in the same conditions. The obtained curves were found to be reproducible.

3. Results

3.1. Microstructure and Mechanical Properties

Figure 3a shows the XRD patterns of the nondeformed sample (N = 0) and ECAP'ed samples (N = 1 to 4). The 222 and 400 reflections of the nondeformed material (N = 0) were not detected, thus indicating a texture of the nondeformed sample. The texture was partially removed after ECAP due to the strain path changes involved in the ECAP process. After ECAP, a pronounced broadening of the X-ray reflections was observed (Figure 3b). This broadening was attributed to the grain refinement and lattice distortions of the ECAP'ed samples. In addition, the broadening of the X-ray reflections made the Kα2 reflection scarcely visible after ECAP. This reflection was well resolved for the nondeformed sample.

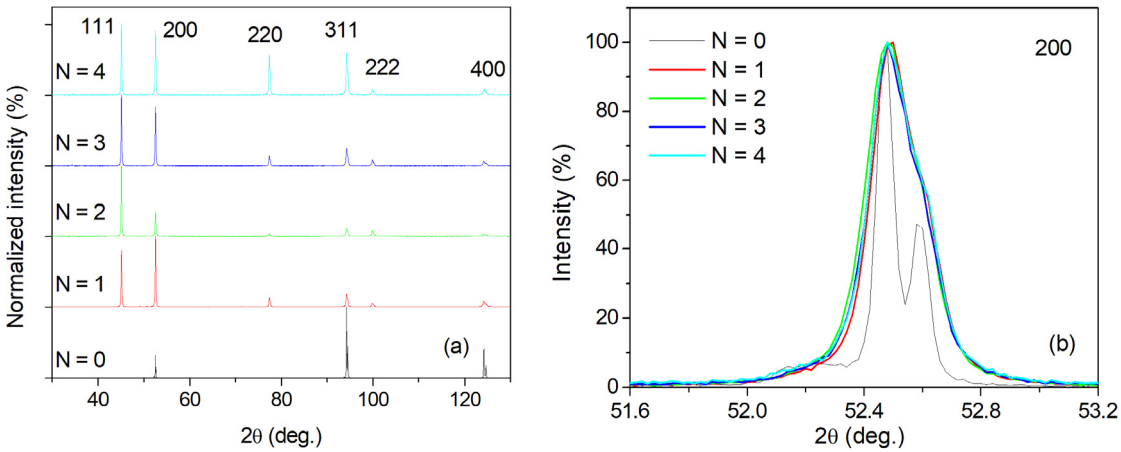

Figure 3. (**a**) XRD patterns and (**b**) the 200 reflection profile of the nondeformed (N = 0) and ECAP'ed (N = 1–4) aluminum samples.

The intensive grain refinement and accumulation of lattice defects such as dislocations during ECAP resulted in a significant strengthening of the deformed alloy, i.e., an increase in the flow stress (Figure 4), and Vickers microhardness was depicted after the ECAP process. The values of the cell size, microstrains, dislocation density, 0.2% flow stress, and Vickers microhardness obtained after the ECAP are reported in Table 1. Significant refinement of the grains was depicted after SPD through the ECAP process. Indeed, the crystallite size attained ~190 nm after the first pass and further decreased to reach ~150 nm after four passes. The lattice distortions continuously increased with the number of passes of the ECAP process. For example, the value of microstrains obtained for N = 1 was 0.08% and increased to 0.15% after four passes.

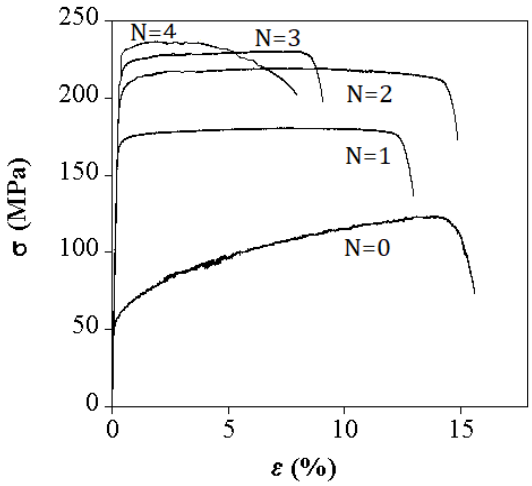

Figure 4. True stress–strain curves of the nondeformed (N = 0) and ECAP'ed (N = 1–4) samples.

Table 1. Crystallite sizes, microstrains, dislocation densities, Vickers microhardness, and 0.2% flow stress values of the aluminum alloy after ECAP.

Number of ECAP Passes N	Crystallite Size (nm)	Microstrains (%)	Dislocations Density ($\times 10^{15}$ m^{-2})	Vickers Microhardness (H_V)	$\sigma_{0.2}$ (MPa)
0	8×10^4	-	-	33	110
1	190	0.08	1.6	60	190
2	185	0.09	2.5	63	210
3	165	0.12	2.6	65	230
4	150	0.15	2.8	76	240

In addition, the ECAP process introduced an increment of dislocation density. Thus, the undeformed (N = 0) aluminum sample should contain a significantly lower dislocation density than the ECAP'ed samples since it was submitted to a prolonged annealing treatment before deformation. It is seen from Table 1 that the highest dislocation density (2.8×10^{15} m^{-2}) and the lowest crystallite size (150 nm) were obtained after four passes. TEM analysis facilitated the obtaining of direct evidence of grain refinement and the accumulation of dislocations after ECAP (Figure 5). The Vickers microhardness reached after one pass (N = 1) became twice as high as the nondeformed (N = 0) sample, and a significant increase in the flow stress at 0.2% was also depicted after the first pass. The highest values were obtained after four passes (Table 1). Ghosh et al. [44] studied the mechanical properties of Al–Zn–Mg–Cu alloys through ECAP after optimizing the outer corner angles through finite element modeling. They depicted an improvement in the hardness and yield strength, by 22% and 18%, respectively, after ECAP. This improvement was attributed to grain refinement and precipitate hardening. In the present work, the improvement of the mechanical properties (H_v and $\sigma_{0.2}$) was by more than 200% after the fourth pass. Therefore, grain refinement was strongly affected by the strain accumulated during the ECAP process. Three stages are typically involved in the intense refinement during SPD [45]: (i) the dislocations are concentrated in high-density shear bands, where the deformation is localized; (ii) these dislocations annihilate at a certain level of strain and rearrange to form small-angle grain boundaries separating the individual crystallites; (iii) the orientation of the crystallites becomes completely random with respect to their neighboring, and a deformation steady state is reached when the rate of the dislocation generation becomes equal to the rate of annihilation. According to the theory of dynamic recovery, internal stresses are reduced during mechanical deformation while also producing more internal stresses (i.e., dislocations). The density of dislocations in a material affects the kinetics of dislocation recovery. That is, the annihilation rate of dislocation increases at

higher strains, which results in smaller crystallite sizes. This would explain the high strains and decreased crystallite sizes obtained in the present work after four passes.

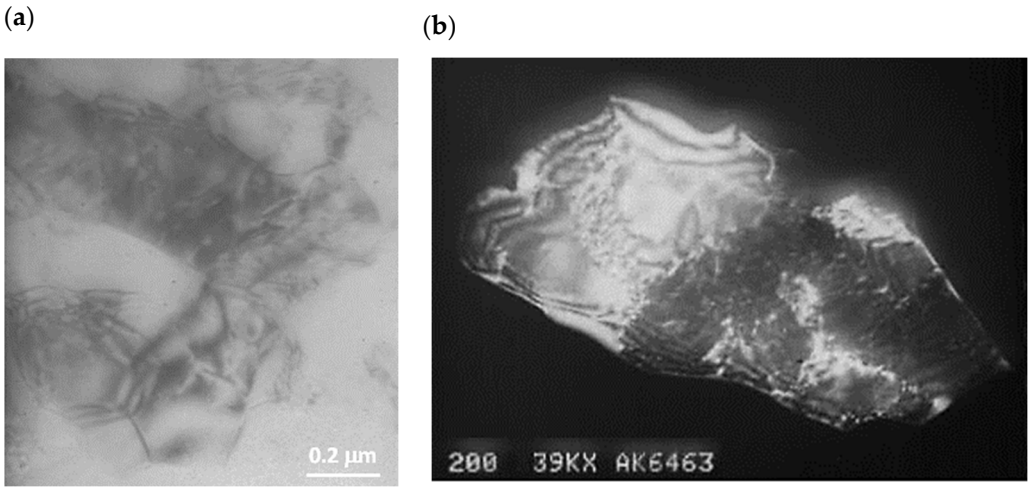

Figure 5. TEM images of the aluminum sample processed by ECAP (N = 4) showing the (**a**) grain refinement and (**b**) accumulation of dislocations after ECAP.

Typical 2D and 3D AFM images of the microstructure of the aluminum samples deformed by ECAP (N = 4) using route A are shown in Figure 6a,b, respectively. The microstructure was relatively homogeneous, and the grain size obtained was ~150 nm in size. This value was slightly higher than that obtained by XRD analysis for the same sample. During SPD, sub-grain boundaries evolve in the grain structures [46], developing coherent crystalline domains [47,48]. The distribution of dislocations may affect the size of these domains. XRD allows the sizes of these coherent domains (crystallite sizes) to be determined. However, AFM (or SEM and TEM) investigations give the grain size distribution from direct observation. This explains the difference in grain size values determined by XRD and AFM. Also, the AFM images reveal the formation of shear bands during the ECAP process. These mesoscopic bands, labeled MB in Figure 6a, are aligned with the shearing plane generated by the ECAP. Similar results were reported for ECAP'ed pure gold [36]. In addition, an examination of the AFM images (Figure 6b) revealed the development of mesoscopic grain boundary sliding (GBS) as proposed by the model of Hahn et al. [28]. In this model, planar interfaces are formed by the migration of grain boundaries. In nanostructured materials, the grain boundary width constitutes a significant fraction of the overall volume of the material, and this favors the formation of planar interfaces [40]. After that, the localized sliding shears lead to macroscopic sliding over dimensions that are significantly greater than the grain size and lead to enhanced strains and superplastic deformation. This is clearly supported by the present AFM images. The occurrence of mesoscopic GBS was established for UFG Cu and Ni with grain sizes of ~220 nm [49], pure gold with a grain size of ~500 nm [36], and pure aluminum with a grain size of 1.3 µm [40] processed by ECAP. However, mesoscopic GBS did not form in a two-phase 2% Al alloy because of the difficulties to achieve local rearrangements of the grain boundaries when two separate phases were present [40]. In the present work, the α-phase, which constitutes a low-volume fraction of the material, apparently did not affect the mesoscopic GBS formation.

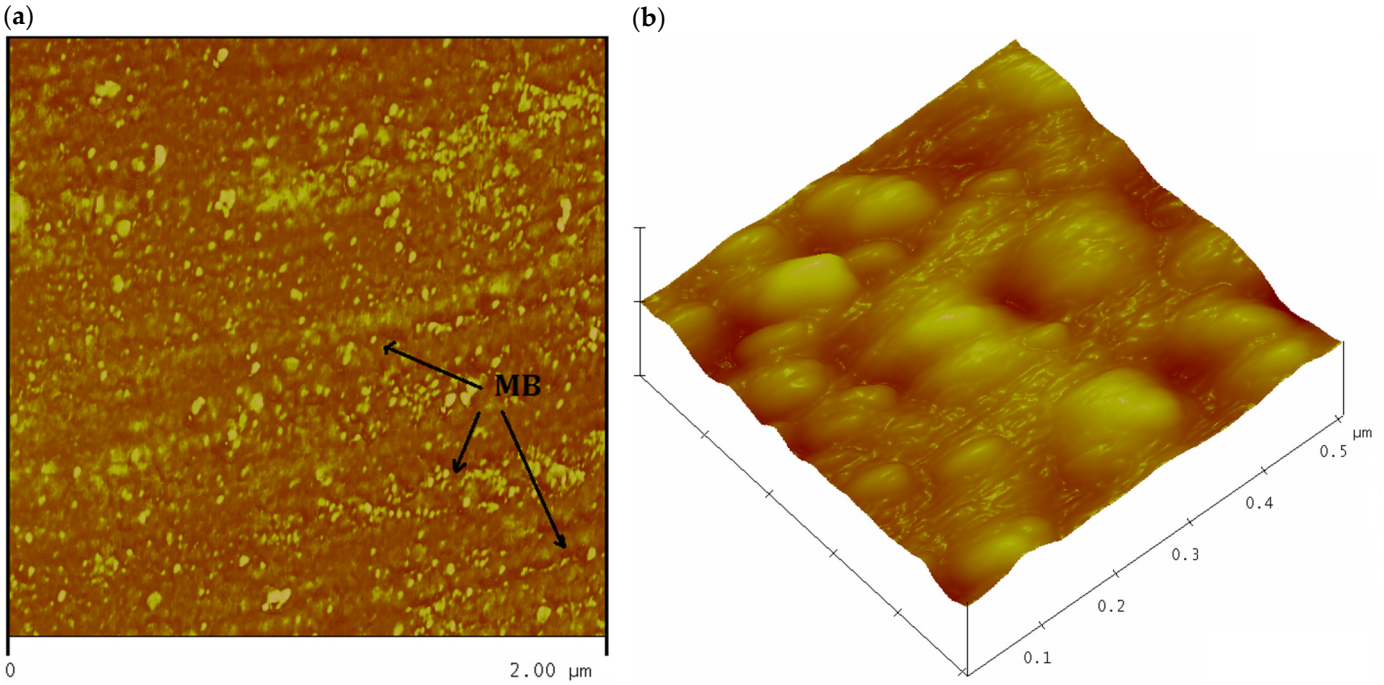

Figure 6. Typical (**a**) 2D and (**b**) 3D AFM images for the aluminum sample processed by ECAP (N = 4). MB: mesoscopic bands.

3.2. Annealing Effect

DSC results of the ECAP'ed (N = 4) material showed main two exothermal peaks at 222 ± 2 °C and 362 ± 2 °C with a total thermal effect of ΔH = 4.35 and 6.5 J/g, respectively (Figure 7). It should be noted that no transformation was detected when two successive heating runs were repeated on the same sample. This indicates irreversible transformations. Other than this, the two peaks were not observed or scarcely visible for the ECAP'ed samples up to N = 3 (results not shown herein). The values of stored energy were lower than those obtained in a cryogenic ball-milled Al-7.6 at% Mg alloy in which recovery occurred during anneals at temperatures between 100 and 230 °C, and recrystallization proceeded at higher temperatures to 370 °C [50]. A slight increase in the microhardness, H_V, and 0.2% flow stress, $\sigma_{0.2}$, of the ECAP'ed material was observed after annealing at 200 °C (Table 2). This might be explained by several microstructure features: (i) Considering the properties of coarse-grained aluminum, the thermal treatment and enhanced diffusivity facilitate the diffusion of impurities toward strained regions around dislocations. The formation of the Cottrell atmosphere decreases the dislocation's mobility, leading to higher Vickers microhardness and flow stress values. (ii) Considering the special behavior of ECAP'ed materials [47], the strengthening of the material after annealing at 200 °C can be attributed to the change of the dislocation cell walls structure from a highly disordered structure to low-angle grain boundaries more resistant than disordered walls. (iii) The pinning of tangled dislocation by the existing fine particles (Figure 8) may result in the improvement of the Vickers microhardness and flow stress.

The peak at 362 °C is in the range of recrystallization temperatures of Al-based alloys [51,52]. In a previous work [53], we demonstrated that after annealing of 1h at a temperature of 400 °C, the ECAP'ed material exhibited a fully recrystallized microstructure consisting of grains ~40 µm in size. This explains the decrease in the ECAP'ed material microhardness H_V and 0.2% flow stress, $\sigma_{0.2}$, at temperatures above 200 °C (Table 2). It should be noted that the microhardness obtained after annealing for 1 h at 400 °C was slightly greater than that of the nondeformed material (N = 0). This was attributed to the lower grain size and redistribution of the α-phase in the aluminum matrix after ECAP, which create a recrystallized structure that differs from that of the nondeformed material.

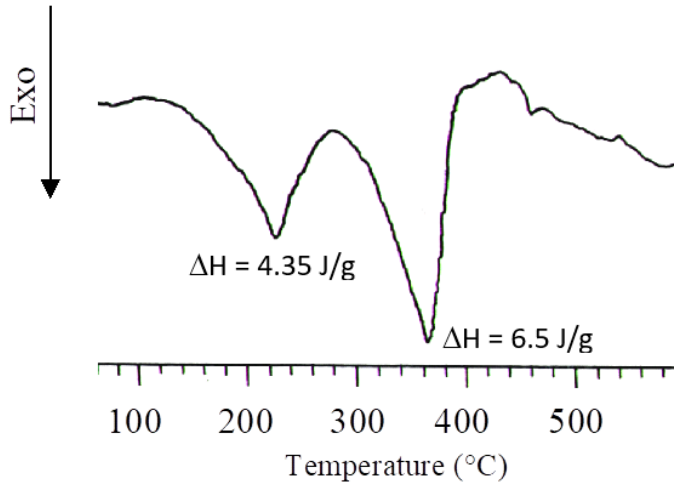

Figure 7. DSC curve of the ECAP'ed (N = 4) aluminum sample.

Table 2. Vickers microhardness and 0.2% flow stress values of the ECAP'ed (N = 1) aluminum alloy at different annealing temperatures.

Temperature (°C)	Vickers Microhardness (H_V)	$\sigma_{0.2}$ (MPa)
25	60	190
200	80	215
370	40	72

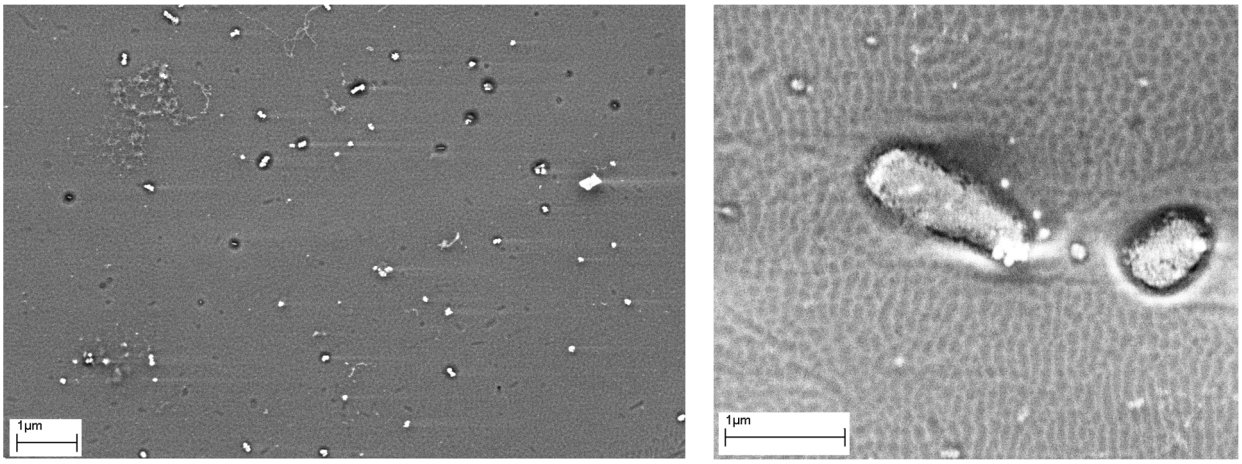

Figure 8. SEM micrographs of the fine precipitates in the ECAP'ed aluminum sample (N = 1). Precipitates can pin the tangled dislocations.

4. Conclusions

XRD, OM, SEM, TEM, and AFM were used to investigate the microstructure of an aluminum alloy containing an iron-rich α-phase deformed by ECAP. Intensive grain refinement and accumulation of strains that resulted in a significant strengthening of the aluminum alloy were observed after ECAP. After four passes, the size of the grains and the dislocation density attained ~150 nm and 2.8 × 10^{15} m^{-2}, respectively. AFM provided direct evidence of the formation of mesoscopic grain boundaries sliding during the ECAP process. A significant increase in the Vickers microhardness and 0.2% flow stress was depicted for the ECAP'ed samples. DSC results showed that the ECAP'ed material (N = 4) exhibited two exothermal peaks at 222 ± 2 °C and 362 ± 2 °C with a total thermal effect of ΔH = 4.35 and 6.5 J/g, respectively. The heat release at the relatively low temperature was attributed to microstructural features such as the diffusion of impurities towards the strain

region around dislocation lines, the change in the dislocation cell wall structure from high disordered structure to low angle grain boundaries, and the pinning of tangled dislocations by the existing fine particles. As a result, a slight increase in the microhardness H_V and 0.2% flow stress of the aluminum alloy was observed after annealing at 200 °C. This is of utmost importance for industrial applications of aluminum alloys at relatively high temperatures since ECAP'ed materials are generally confronted with intensive softening after annealing. The second peak was attributed to grain growth. Indeed, a significant softening was observed by annealing at temperatures higher than 200 °C, which was attributed to grain growth.

Author Contributions: A.K. was involved in the methodology, experimental investigation, supervision, and writing and editing of the work. I.S. was involved in ensuring resources, data curation, and formal analysis of the work. All authors have read and agreed to the published version of the manuscript.

Funding: This research was funded by the Deanship of Scientific Research at King Khalid University, Saudi Arabia, grant number GRP/87/44.

Data Availability Statement: Not available.

Acknowledgments: The authors extend their appreciation to the Deanship of Scientific Research at King Khalid University, Saudi Arabia, for funding this work through the General Research Project under grant number GRP/87/44.

Conflicts of Interest: The authors declare no conflict of interest.

References

1. Wetscher, F.; Vorhauer, A.; Pippan, R. Strain hardening during high pressure torsion deformation. *Mater. Sci. Eng. A* **2005**, *410–411*, 213–216. [CrossRef]
2. Kawasaki, M.; Han, J.K.; Lee, D.H.; Jang, J.; Langdon, T.G. Fabrication of nanocomposites through diffusion bonding under high-pressure torsion. *J. Mater. Res.* **2018**, *33*, 2700–2710. [CrossRef]
3. Kunčická, L.; Jambor, M.; Král, P. High pressure torsion of copper; effect of processing temperature on structural features, microhardness and electric conductivity. *Materials* **2023**, *16*, 2738. [CrossRef]
4. Charfeddine, S.; Zehani, K.; Bessais, L.; Korchef, A. Microstructure characterization of an aluminium alloy processed by milling followed by spark plasma sintering. *Crys. Res. Technol.* **2018**, *53*, 1700137. [CrossRef]
5. Daniyan, I.A.; Tlhabadira, I.; Mpofu, K.; Adeodu, A.O. Process design and optimization for the milling operation of aluminum alloy (AA6063 T6). Mater. *Today Proc.* **2021**, *38*, 536–543. [CrossRef]
6. Segal, V.M.; Reznikov, V.I.; Drobyshevskii, A.E.; Kopylov, V.I. Plastic metal working by simple shear. *Izv. Akad. Nauk. SSSR Met.* **1981**, *1*, 115–123. [CrossRef]
7. Bednarczyk, W.; Wątroba, M.; Kawałko, J.; Bała, P. Can zinc alloys be strengthened by grain refinement? A critical evaluation of the processing of low-alloyed binary zinc alloys using ECAP. *Mater. Sci. Eng. A* **2019**, *748*, 357–366. [CrossRef]
8. Volokitina, I.; Bychkov, A.; Volokitin, A.; Kolesnikov, A. Natural aging of aluminum alloy 2024 after severe plastic deformation. *Metallogr. Microstruct. Anal.* **2023**, *12*, 564–566. [CrossRef]
9. Sagar, K.G.; Suresh, P.M.; Sampathkumaran, P. Tribological studies on aluminum beryl composites subjected to ECAP process. *Wear* **2023**, *523*, 204775. [CrossRef]
10. El-Garaihy, W.H.; BaQais, A.; Alateyah, A.I.; Alsharekh, M.F.; Alawad, M.O.; Shaban, M.; Alsunaydih, F.N.; Kamel, M. The impact of ECAP parameters on the structural and mechanical behavior of pure Mg: A combination of experimental and machine learning approaches. *Appl. Sci.* **2023**, *13*, 6279. [CrossRef]
11. Shin, D.H.; Park, K.T. Ultrafine grained steels processed by equal channel angular pressing. *Mater. Sci. Eng. A* **2005**, *410–411*, 299–302. [CrossRef]
12. Bodyakova, A.; Tkachev, M.; Pilipenko, A.; Belyakov, A.; Kaibyshev, R. Effect of deformation methods on microstructure, texture, and properties of a Cu–Mg alloy. *Mater. Sci. Eng. A* **2023**, *876*, 145126. [CrossRef]
13. Zhang, L.; Liu, C.Y.; Xie, H.Y. Hall-Petch relation and grain boundary slipping in Al–Mg–Sc alloys with fine equiaxed grain structure. *Mater. Charact.* **2022**, *194*, 112472. [CrossRef]
14. Terhune, S.D.; Swicher, D.L.; Ishi, K.O.; Horita, Z.; Langdon, T.G.; McNelly, T.R. An investigation of microstructure and grain-boundary evolution during ECA pressing of pure aluminum. *Metall. Mater. Trans. A* **2002**, *33*, 2173. [CrossRef]
15. Tang, L.; Peng, X.; Huang, J.; Ma, A.; Deng, Y.; Xu, G. Microstructure and mechanical properties of severely deformed Al–Mg–Sc–Zr alloy and their evolution during annealing. *Mater Sci. Eng. A* **2019**, *754*, 295–308. [CrossRef]
16. Damavandi, E.; Nourouzi, S.; Rabiee, S.M.; Jamaati, R. Effect of ECAP on microstructure and tensile properties of A390 aluminum alloy. *Trans. Nonferrous Met. Soc. China* **2019**, *29*, 931–940. [CrossRef]

17. Nakashima, K.; Horita, Z.; Nemoto, M.; Langdon, T.G. Influence of channel angle on the development of ultrafine grains in equal-channel angular pressing. *Acta Mater.* **1998**, *46*, 1589–1599. [CrossRef]
18. Kawasaki, M.; Horita, Z.; Nemoto, M.; Langdon, T.G. Microstructural evolution in high purity aluminum processed by ECAP. *Mater. Sci. Eng. A* **2009**, *524*, 143–150. [CrossRef]
19. Skrotzki, W.; Scheerbaum, N.; Oertel, C.G.; Brokmeier, H.G.; Suwas, S.; Tóth, L.S. Texture Formation during ECAP of Aluminum Alloy AA 5109. Mater. *Sci. Forum* **2006**, *503–504*, 99–106. [CrossRef]
20. Xue, D.; Wei, W.; Wen, S.; Wu, X.; Shi, W.; Zhou, X.; Gao, K.; Huang, H.; Nie, Z. Microstructural evolution of Al-Mg-Er-Zr alloy by equal channel angular extrusion at room temperature. *Mater. Lett.* **2023**, *3341*, 133759. [CrossRef]
21. Sitdikov, O.; Avtokratova, E.; Markushev, M.; Sakai, T. Structural characterization of binary Al-Cu alloy processed by equal channel angular pressing at half of the melting point. *Metall. Mater. Trans. A* **2023**, *54*, 505–525. [CrossRef]
22. Ghosh, A.; Ghosh, M.; Gudimetla, K.; Kalsar, R.; Kestens, L.A.; Kondaveeti, C.S.; Singh Pugazhendhi, B.; Ravisankar, B. Development of ultrafine grained Al–Zn–Mg–Cu alloy by equal channel angular pressing: Microstructure, texture and mechanical properties. *Arch. Civ. Mech. Eng.* **2020**, *20*, 7. [CrossRef]
23. Huang, S.J.; Subramani, M.; Borodianskiy, K.; Immanuel, P.N.; Chiang, C.C. Effect of equal channel angular pressing on the mechanical properties of homogenized hybrid AZ61 magnesium composites. *Mater. Today Commun.* **2023**, *34*, 104974. [CrossRef]
24. Dyakonov, G.S.; Raab, G.I.; Pesin, M.V.; Polyakov, A.V.; Semenova, I.P.; Valiev, R.Z. Superplastic-like behavior and enhanced strength of a two-phase titanium alloy with ultrafine grains. *Adv. Eng. Mater.* **2022**, *24*, 2101592. [CrossRef]
25. Mabuchi, M.; Higashi, K. Mechanical properties of pure aluminium processed by equal channel angular extrusion. *J. Mater. Sci. Lett.* **1998**, *17*, 215–217. [CrossRef]
26. Verlinden, B.; Popović, M. Influence of Cu on the Mechanical Properties of an Al-4.4 wt% Mg Alloy after ECAP. *Mater. Sci. Forum* **2006**, *503–504*, 107–112. [CrossRef]
27. Schiøtz, J.; Vegge, T.; Di Tolla, F.D.; Jacobsen, K.W. Atomic-scale simulations of the mechanical deformation of nanocrystalline metals. *Phys. Rev. B* **1999**, *60*, 11971–11983. [CrossRef]
28. Hahn, H.; Mondal, P.; Padmanabhan, K.A. Plastic deformation of nanocrystalline materials. *J. Nanostruct.* **1997**, *9*, 603–606. [CrossRef]
29. Valiev, R.Z.; Krasilnikov, N.A.; Tsenev, N.K. Plastic deformation of alloys with submicron-grained structure. *Mater. Sci. Eng. A* **1991**, *137*, 35–40. [CrossRef]
30. Lifshitz, I.M. On the theory of diffusion-viscous flow of polycrystalline bodies. *Sov. Phys. Jetp-Ussr* **1963**, *17*, 909–920.
31. Rachinger, W.A. Relative grain translations in the plastic flow of aluminium. *J. Inst. Met.* **1952**, *81*, 33.
32. Furukawa, M.; Horita, Z.; Nemoto, M.; Langdon, T.G. The significance of the Hall-Petch relationship in ultra-fine grained materials: Matériaux à grains ultra-fins produits par hypercorroyage. In *Annales de Chimie*; Lavoisier: Cachan, France, 1996; Volume 21, pp. 493–502.
33. Chokshi, A.H.; Rosen, A.; Karch, J.; Gleiter, H. On the validity of the hall-petch relationship in nanocrystalline materials. *Scr. Metall.* **1989**, *23*, 1679–1683. [CrossRef]
34. Nieh, T.G.; Wadsworth, J. Hall-petch relation in nanocrystalline solids. *Scr. Metall. Mater.* **1991**, *25*, 955–958. [CrossRef]
35. Valiev, R.Z.; Korznikov, A.V.; Mulyukov, R.R. Structure and properties of ultrafine-grained materials produced by severe plastic deformation. *Mater. Sci. Eng. A* **1993**, *168*, 141–148. [CrossRef]
36. Gubicza, J.; Chinh, N.Q.; Szommer, P.; Vinogradov, A.; Langdon, T.G. Microstructural characteristics of pure gold processed by equal-channel angular pressing. *Scr. Mater.* **2007**, *56*, 947–950. [CrossRef]
37. Alipour, S.; Vafaeenezhad, H.; Fesahat, M.; Yazdi, A.; Mousavi-Khoshdel, S.M.; Soltanieh, M. Electrochemical behavior of ECAP-processed Sn–5Sb alloy. *J. Mater. Res. Technol.* **2023**, *23*, 5193–5211. [CrossRef]
38. Hussainova, I.; Kommel, L.; Lohmus, R.; Volobujeva, O. Microscopic characterization of surface morphology of nanostructured copper. *Rev. Adv. Mater. Sci.* **2005**, *10*, 266–271.
39. Kimura, H.; Kojima, Y.; Akiniwa, Y.; Tanaka, K.; Ishida, T. Fatigue damage mechanism of nanocrystals in ECAP-processed copper investigated by EBSD and AFM hybrid methods. *Key Eng. Mater.* **2007**, *340*, 943–948. [CrossRef]
40. Huang, Y.; Langdon, T.G. Characterization of deformation processes in a Zn-22% Al alloy using atomic force microscopy. *J. Mater. Sci.* **2002**, *37*, 4993–4998. [CrossRef]
41. Iwahashi, Y.; Wang, J.; Horita, Z.; Nemoto, M.; Langdon, T.G. Principle of equal-channel angular pressing for the processing of ultra-fine grained materials. *Scr. Mater.* **1996**, *35*, 143–146. [CrossRef]
42. Langford, J.I. National Institute of Standards and Technology Special Publication 846. In Proceedings of the International Conference Accuracy in Powder Diffraction II, NIST, Gaithersburg, MD, USA, 26–29 May 1992; pp. 241–244.
43. Rebhi, A.; Maklouf, T.; Njah, N.; Champion, Y.; Couzinié, J.P. Characterization of aluminium processed by equal angular extrusion: Effect of processing route. *Mater. Charact.* **2009**, *60*, 1489–1495. [CrossRef]
44. Ghosh, A.; Das, K.; Eivani, A.R.; Mohammadi, H.; Vafaeenezhad, H.; Murmu, U.K.; Jafarian, H.R.; Ghosh, M. Development of mechanical properties and microstructure for Al–Zn–Mg–Cu alloys through ECAP after optimizing the outer corner angles through FE modeling. *Arch. Civ. Mech. Eng.* **2023**, *23*, 78. [CrossRef]
45. Bate, P.S.; Humphreys, F.J.; Ridley, N.; Zhang, B. Microstructure and texture evolution in the tension of superplastic Al–6Cu–0.4 Zr. *Acta Mater.* **2005**, *53*, 3059–3069. [CrossRef]

46. Ito, Y.; Horita, Z. Microstructural evolution in pure aluminum processed by high-pressure torsion. *Mater. Sci. Eng.* **2009**, *503*, 32–36. [CrossRef]
47. Valiev, R.Z.; Islamagaliev, R.K.; Alexandrov, I.V. Bulk nanostructured materials from severe plastic deformation. *Prog. Mater. Sci.* **2000**, *45*, 103–189. [CrossRef]
48. Zangiabadi, A.; Kazeminezhad, M. Development of a novel severe plastic deformation method for tubular materials: Tube Channel Pressing (TCP). *Mater. Sci. Eng.* **2011**, *528*, 5066–5072. [CrossRef]
49. Vinogradov, A.; Hashimoto, S.; Patlan, V.; Kitagawa, K. Atomic force microscopic study on surface morphology of ultra-fine grained materials after tensile testing. *Mater. Sci. Eng. A* **2001**, *319*, 862–866. [CrossRef]
50. Zhou, F.; Liao, X.Z.; Zhu, Y.T.; Dallek, S.; Lavernia, E.J. Microstructural evolution during recovery and recrystallization of a nanocrystalline Al-Mg alloy prepared by cryogenic ball milling. *Acta Mater.* **2003**, *51*, 2777–2791. [CrossRef]
51. Zaidi, M.A.; Sheppard, T. Effect of high-temperature soak and cooling rate on recrystallization behaviour of two Al-Mg alloys (AA 5252 and AA 5454). *Met. Technol.* **1984**, *11*, 313–319. [CrossRef]
52. Koken, E.; Embury, J.D.; Ramachandran, T.R.; Malis, T. Recrystallization at shear bands in Al-Mg. *Scr. Metall.* **1988**, *22*, 99–103. [CrossRef]
53. Korchef, A.; Champion, Y.; Njah, N. X-ray diffraction analysis of aluminium containing Al_8Fe_2Si precipitates processed by equal channel angular pressing. *J. Alloys Compd.* **2007**, *427*, 176–182. [CrossRef]